# Modeling the influence of pulsed GMAW parameters on the weld bead geometry of structural steel

***Jure Krolo*[1], *Mislav Prcela*[1], *Petar Ljumović*[1] *and Nina Mucić*[1]**

*1) Faculty of Electrical Engineering, Mechanical Engineering and Naval Architecture, University of Split, Ruđera Boškovića 32, 21000 Split, Croatia*

*Corresponding author: jkrolo@fesb.hr*

*Original Scientific Paper*

**Abstract:** The main objective of this work is to quantitatively model the combined influence of arc correction, contact tip to work distance (CTWD), and welding travel speed on weld bead geometry in pulsed GMAW of structural steel. A structured Box–Behnken experimental design combined with response surface methodology was employed to evaluate main and interaction effects of the selected parameters on bead width, reinforcement height, penetration depth, heat input, and measured voltage. The study aims to establish statistically validated regression models capable of describing coupled thermo-electrical–geometrical relationships governing bead formation. Particular emphasis is placed on identifying interaction-driven penetration behavior, which cannot be explained solely by heat input magnitude. The developed models provide predictive capability for systematic parameter tuning, improved process understanding, and enhanced control of weld bead geometry in mechanized and semi-automated MAG welding applications.

**Keywords:** *pulsed MAG welding; weld bead geometry; design of experiments; response surface methodology; wire arc additive manufacturing (WAAM)*

## 1. Introduction

Gas metal arc welding (GMAW), commonly referred to as MIG/MAG welding, is one of the most widely applied arc welding processes in industrial practice due to its high productivity, process stability, and suitability for mechanization and automation. In this process, an electric arc is established between a continuously fed consumable wire electrode and the workpiece, while the arc and molten metal are protected from atmospheric contamination by a shielding gas [1]. Owing to these characteristics, MIG/MAG welding is extensively used in semi-automated, automated, and robotic welding systems [1], [2]. Classical welding literature indicates that weld bead geometry in MIG/MAG welding is primarily governed by arc stability, heat input distribution, and metal transfer behavior [1]. These phenomena are strongly affected by process parameters such as arc length control, contact tip to work distance (CTWD), and welding travel speed. Stable arc behavior promotes uniform heat distribution and consistent droplet transfer, which are essential for reproducible bead geometry and minimized geometric irregularities [1], [2]. CTWD is recognized as a key parameter influencing electrical resistance heating of the wire and, consequently, welding current and heat input. Increasing CTWD generally reduces current and penetration, affecting bead width and profile shape, while excessively small CTWD may lead to arc instability and excessive heat input [1]. Welding travel speed directly controls the energy input per unit length; lower speeds result in wider beads due to increased heat input, whereas higher speeds reduce bead width and may increase the risk of lack of fusion or geometric instability [1], [2]. Modern pulsed GMAW power sources incorporate additional synergic control parameters, such as arc correction, which enable fine adjustment of arc length and metal transfer behavior relative to nominal synergic settings. According to general conclusions reported in welding literature, such arc control parameters play a critical role in stabilizing the arc and controlling heat input distribution, particularly under mechanized and semi-automated conditions [2]. However, their combined influence with CTWD and welding travel speed on bead geometry has not been sufficiently quantified. Although this study is conducted within the framework of pulsed GMAW

welding, the investigated bead formation mechanisms are directly relevant to wire arc additive manufacturing (WAAM), where component fabrication is based on the controlled deposition of successive weld beads. In WAAM processes, the geometry and stability of the first deposited bead are of particular importance, as they strongly influence subsequent layer formation, dimensional accuracy, and overall process stability. Consequently, the modeling of single-bead geometry addressed in this work represents not only a welding-related investigation but also a fundamental basis for parameter selection and process control in WAAM-based manufacturing. Previous studies on wire arc additive manufacturing have shown that the geometry of individual deposited beads has a decisive influence on the stability and dimensional accuracy of multi-layer structures. Dinovitzer et al. demonstrated that process parameters such as arc characteristics and travel speed significantly affect bead geometry and microstructure in WAAM, emphasizing that reliable modeling of single-bead formation is a fundamental prerequisite for process optimization [3]. Kim *et al.* investigated robotic MAG ($CO_2$) welding of structural steel and showed that welding current has a strong positive influence on bead penetration, while welding travel speed has a strong negative effect due to its inverse relationship with heat input per unit length. An increase in travel speed led to a pronounced reduction in penetration even when other parameters were kept constant. The authors concluded that penetration control in automated MAG welding requires simultaneous optimization of interacting process parameters rather than independent adjustment [4]. Manikya Kanti and Srinivasa Rao studied pulsed GMAW of steel plates and demonstrated that bead penetration and bead shape are governed by peak current, wire feed rate, and welding travel speed, with welding speed primarily controlling heat input and penetration. Pulse-related parameters significantly affected metal transfer stability and bead convexity. The authors concluded that bead geometry in pulsed GMAW is governed by nonlinear interactions between parameters, necessitating coupled experimental and modeling approaches [5]. Due to the complex interactions between multiple welding parameters, systematic statistical modeling approaches are commonly applied to describe and optimize bead geometry in arc-based deposition processes. Kumar et al. employed response surface methodology to establish predictive relationships between welding parameters and deposited bead geometry, showing that structured experimental designs enable efficient evaluation of parameter interactions and support systematic process optimization [6]. Response surface methodology (RSM) is widely applied for modeling and optimization of manufacturing processes, as it enables the development of empirical regression models and visualization of parameter interactions [7], [8]. Among available experimental designs, the Box–Behnken design represents an efficient second-order design that allows the construction of quadratic response models with a reduced number of experimental runs compared to full factorial designs. Therefore, the objective of this study is to investigate the influence of arc correction, contact tip to work distance, and welding travel speed on weld bead geometry using a Box–Behnken experimental design combined with response surface methodology. The applied approach enables quantitative evaluation of main effects and interaction effects, as well as the identification of optimal parameter combinations for achieving stable bead geometry. The obtained results are intended to support improved process understanding, enhanced control of weld bead formation, and increased applicability of pulsed MAG welding in automated and semi-automated deposition processes. Unlike most existing studies focusing on individual welding parameters, this work evaluates their combined influence using a structured experimental framework, thereby providing a more realistic representation of semi-automated MAG welding conditions. By integrating electrical (voltage), thermal (heat input), and geometrical (bead dimensions and penetration) responses within a statistically validated response surface framework, this study provides a physically consistent and experimentally supported understanding of parameter interactions in pulsed GMAW, offering robust, easily transferable, and directly applicable guidelines for real industrial welding and WAAM-based manufacturing systems.

## 2. Materials and methods

The experimental investigation was conducted using a structured design of experiments (DoE) approach in order to evaluate the influence of selected pulsed MAG welding parameters on the geometry of the weld bead. Three process parameters were considered as input factors, each varied at three discrete levels, as presented in Table 1. Factor A represents the arc correction parameter, expressed as a percentage, which directly influences arc stability and heat input distribution. The arc correction was varied at levels of 0%, 30%, and 60%. Factor B corresponds to the contact tip to work distance (CTWD), defined as the distance between the contact tip and the workpiece, and was set to 10 mm, 15 mm, and 20 mm. Factor C denotes the welding travel speed, varied at levels of 4.0 mm/s, 6.5 mm/s, and 9.0 mm/s. A total of seventeen experimental runs were performed, including repeated trials at the central parameter combination in order to evaluate process stability and experimental repeatability. The order of experiments was randomized to minimize the influence of uncontrolled variables. All other welding parameters and environmental conditions were kept constant throughout the experimental campaign.

***Table 1.*** *Design of experiments – process parameters*

| Run | A: Arc Correction (%) | B: CTWD (mm) | C: Welding Speed (mm/s) |
|---|---|---|---|
| 1 | 0.00 | 20.00 | 6.50 |
| 2 | 30.00 | 15.00 | 6.50 |
| 3 | 0.00 | 15.00 | 4.00 |
| 4 | 30.00 | 10.00 | 9.00 |
| 5 | 30.00 | 20.00 | 4.00 |
| 6 | 0.00 | 15.00 | 9.00 |
| 7 | 30.00 | 15.00 | 6.50 |
| 8 | 30.00 | 15.00 | 6.50 |
| 9 | 30.00 | 20.00 | 9.00 |
| 10 | 30.00 | 15.00 | 6.50 |
| 11 | 30.00 | 10.00 | 4.00 |
| 12 | 60.00 | 10.00 | 6.50 |
| 13 | 60.00 | 15.00 | 4.00 |
| 14 | 0.00 | 10.00 | 6.50 |
| 15 | 60.00 | 20.00 | 6.50 |
| 16 | 30.00 | 15.00 | 6.50 |
| 17 | 60.00 | 15.00 | 9.00 |

The welding experiments were carried out using a gas metal arc welding (GMAW) system. A Daihen Varstroj WB-P500L welding power source was employed as the arc heat source for all deposition trials. Table 2 shows welding parameters which were held constant during experiments.

***Table 2.*** *Constant welding parameters used for bead deposition*

| Welding parameters | |
|---|---|
| **Nominal electric current (A)** | 250 |
| **Work mode** | DCEP |
| **Pulse welding** | yes |
| **Shielding gas** | Ar (82%) + $CO_2$ (18%) |
| **Gas flow (L / min)** | 20 |
| **Electrode type** | ϕ 1.2 mm mild steel |
| **Filler material** | ER70S-6 |

The power source was operated in pulsed GMAW mode, enabling controlled metal transfer and improved arc stability during deposition. The welding torch was mounted on a mechanized motion system to ensure repeatable and stable deposition conditions. Substrate was 12 mm **thick** carbon steel plate designated as S235JR+AR. Testo 770-3 was used to measure voltage during process. After deposition, specimens were cut from each deposited bead using a metallographic cutter, Buehler Delta. The specimens were subsequently ground and polished using a Struers Labopol-Z metallographic polishing system. Grinding was performed using 1200 grit SiC paper, followed by a one-stage polishing with 9 µm alumina. For optical microscopy, the specimens were etched with 6% nital solution (6 vol.% nitric acid in ethanol) for 60 s. Optical microscopy was performed utilizing an Olympus SZ61 optical stereomicroscope. Digital images of the prepared specimens were analyzed using the open-source software ImageJ. The heat input was determined from the welding current, arc voltage, process efficiency, and travel speed according to the standard relationship given in Equation (1).

$$HI = \frac{I \cdot V \cdot \eta}{v \cdot 1000} \tag{1}$$

where $I$ is the welding current (A), $V$ is the arc voltage (V), $\eta$ is the process efficiency factor, and $v$ is the welding travel speed (mm/s). The heat input is expressed in kJ/mm. For the GMAW process, the process efficiency factor (η) was assumed to be 0.80, which is a commonly accepted value in welding literature [9].

## 3. Results and discussion

The measured and calculated response variables obtained during the experimental campaign are summarized in Table 3, while the corresponding combinations of process parameters are defined in Table 1. The results indicate a clear dependence of weld bead geometry on the selected pulsed GMAW parameters, particularly welding travel speed, arc-related control, and heat input. The figure 1 presents the top-view appearance of the deposited weld beads corresponding to the seventeen experimental runs defined in Table 1, illustrating the visible influence of arc correction, CTWD, and welding travel speed on bead morphology and surface stability.



***Figure 1.*** *Overview of deposited weld bead surfaces for all experimental runs (1–17) according to the Box–Behnken design*

Figure 2 presents representative cross-sectional macrographs of selected weld beads (Runs 6, 5, 11, 9, 7, and 12), illustrating characteristic differences in fusion geometry, penetration depth, and reinforcement as a function of arc correction, CTWD, and welding speed. The observed variations confirm that weld bead morphology is governed by the combined interaction of process parameters rather than by heat input alone. Run 6, characterized by the lowest heat input, exhibits a comparatively shallow penetration profile and moderate reinforcement, reflecting the limited thermal

energy per unit length and reduced molten pool development. In contrast, Run 5, associated with one of the highest heat input conditions, demonstrates a substantially deeper and wider fusion zone, accompanied by increased bead reinforcement, indicating enhanced energy transfer and extended thermal diffusion into the base material. Run 11 shows one of the highest measured penetration depths, despite not corresponding to the absolute maximum heat input. This behavior can be attributed to the reduced CTWD and more concentrated arc conditions, which promote deeper energy penetration and a more vertically oriented fusion profile. Conversely, Run 9, combining higher travel speed with increased CTWD, produces a flatter bead morphology and reduced penetration, consistent with lower effective energy density and broader arc dispersion. The central parameter combination (Run 7) results in a relatively balanced bead geometry with moderate penetration and reinforcement, indicating stable arc behavior under intermediate conditions. Run 12 further demonstrates that elevated arc correction contributes to improved arc stability and uniform fusion geometry, while maintaining controlled reinforcement levels. Overall, the macrostructural observations support the statistical trends obtained through response surface modeling, confirming that penetration depth and bead geometry are strongly influenced by the interaction between CTWD and arc-related parameters, whereas welding speed primarily governs heat input per unit length.

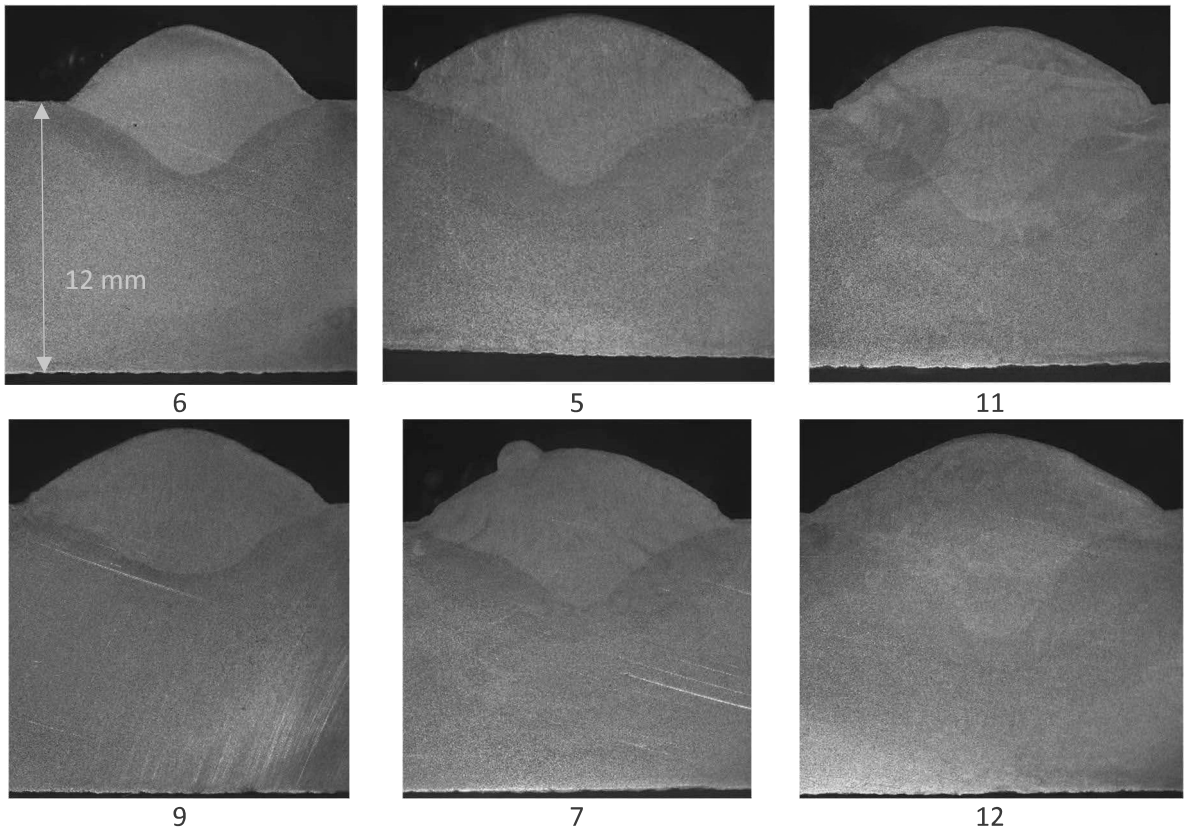



***Figure 2.*** *Representative selected weld bead cross-sections corresponding to extreme and central parameter combinations in the Box–Behnken design*

As shown in Table 3, bead width varied between 11.47 mm and 17.83 mm, while bead reinforcement height ranged from 2.45 mm to 4.08 mm. The measured depth of penetration exhibited a wider variation, from 2.90 mm to 5.42 mm, indicating a pronounced influence of process parameter combinations on fusion behavior. The calculated heat input values ranged from 0.53 kJ/mm to 1.58 kJ/mm, reflecting the combined influence of arc voltage and welding travel speed. In general, higher heat input conditions were associated with increased bead width and deeper fusion zones, as observed in Runs 5 and 13. However, penetration depth did not increase strictly proportionally with heat input in all cases. For example, Runs 11 and 12 exhibited the highest penetration depths (above 5 mm), despite not corresponding to the absolute maximum heat input values. This suggests that arc

concentration effects, influenced by CTWD and arc correction, play a significant role in controlling effective energy density within the molten pool. Lower heat input conditions, particularly those associated with higher welding speeds, resulted in narrower beads and reduced penetration, as demonstrated by Run 6 and Run 9. Nevertheless, certain intermediate parameter combinations (e.g., Run 4 and Run 14) produced relatively deep penetration despite moderate heat input, further confirming that weld bead geometry cannot be attributed to a single governing variable. Overall, the results indicate that welding speed primarily governs the global heat input per unit length, whereas CTWD and arc correction influence the distribution and concentration of thermal energy. Consequently, weld bead geometry in pulsed GMAW is determined by the combined and interacting effects of multiple process parameters, which justifies the application of response surface methodology for systematic modeling and optimization.

***Table 3.*** *Measured and calculated response variables for pulsed GMAW experiments*

| Run | Measured voltage (V) | Bead width (mm) | Bead height (mm) | Heat input (kJ/mm) | Depth of penetration (mm) |
|---|---|---|---|---|---|
| 1 | 27.072 | 12.58 | 3.52 | 0.832985 | 3.42 |
| 2 | 29.45 | 13.53 | 3.30 | 0.906154 | 3.84 |
| 3 | 26.024 | 14.57 | 3.82 | 1.301200 | 3.67 |
| 4 | 26.89 | 13.63 | 3.07 | 0.597556 | 4.39 |
| 5 | 28.934 | 16.68 | 3.55 | 1.446700 | 4.27 |
| 6 | 23.83 | 11.53 | 3.07 | 0.529556 | 3.28 |
| 7 | 27.80 | 13.93 | 2.97 | 0.855385 | 3.92 |
| 8 | 27.89 | 13.98 | 2.97 | 0.858154 | 4.08 |
| 9 | 30.45 | 12.31 | 2.52 | 0.676667 | 2.9 |
| 10 | 28.32 | 12.55 | 3.45 | 0.871385 | 4.27 |
| 11 | 26.14 | 15.02 | 4.08 | 1.307000 | 5.34 |
| 12 | 30.917 | 15.25 | 3.32 | 0.951292 | 5.42 |
| 13 | 31.615 | 17.83 | 3.43 | 1.580750 | 4.9 |
| 14 | 21.867 | 11.47 | 3.73 | 0.672831 | 4.21 |
| 15 | 32.719 | 14.90 | 3.03 | 1.006740 | 3.2 |
| 16 | 28.375 | 14.20 | 2.98 | 0.873077 | 4.26 |
| 17 | 31.661 | 13.67 | 2.45 | 0.703578 | 3.73 |

The statistical results summarized in Table 4 confirm the adequacy and significance of the developed response surface models. All investigated responses exhibited statistically significant models with high *F*-values and *p*-values below 0.0001, indicating that the observed variations are not caused by random experimental noise. For bead geometry, welding speed (C) and arc correction (A) were identified as the dominant controlling factors. In the case of bead width, welding speed showed the strongest contribution ($p < 0.0001$), followed by arc correction, while CTWD did not exhibit statistical significance in the linear model. A similar trend was observed for bead height, where all three factors were significant, although welding speed demonstrated the highest *F*-value, confirming its governing influence on reinforcement formation. Heat input was predominantly controlled by welding speed, as expected from its direct involvement in the heat input equation, with additional contributions from arc correction and CTWD. The presence of a significant quadratic term ($C^2$) indicates slight curvature effects within the investigated design space. The model demonstrated excellent goodness-of-fit ($R^2 \approx 0.99$), confirming strong predictive capability. Measured voltage was primarily influenced by arc correction and CTWD, whereas welding speed showed no statistically significant effect, which is consistent with the physical nature of voltage control in pulsed GMAW. For depth of penetration, all three factors were statistically significant, with CTWD and welding speed exhibiting the strongest influence. Additionally, a significant interaction term (A×B) was detected, indicating that the combined

effect of arc correction and CTWD contributes to penetration behavior beyond their individual linear effects. Importantly, all models exhibited non-significant lack of fit ($p > 0.05$), confirming that the developed regression equations adequately describe the experimental data within the investigated parameter range. The close agreement between adjusted and predicted $R^2$ values further supports the robustness and reliability of the models for process analysis and optimization. The repeated central point experiments showed minimal variation, confirming good process stability and repeatability under intermediate parameter settings.

***Table 4.*** *Analysis of variance (ANOVA) results and model adequacy statistics for bead geometry and thermal responses*

| Response | **Model *F*** | ***p*-value** | **Significant terms** | **$R^2$** | **Adj $R^2$** | **Pred $R^2$** | **Lack of fit** |
|---|---|---|---|---|---|---|---|
| Bead width | 20.69 | <0.0001 | A, C | 0.8268 | 0.7868 | 0.6860 | n.s. |
| Bead height | 24.08 | <0.0001 | A, B, C | 0.8475 | 0.8123 | 0.7683 | n.s. |
| Heat input | 340.29 | <0.0001 | A, B, C, $C^2$ | 0.9913 | 0.9883 | 0.9793 | n.s. |
| Voltage | 58.92 | <0.0001 | A, B | 0.9315 | 0.9157 | 0.8700 | n.s. |
| Penetration | 29.71 | <0.0001 | A, B, C, AB | 0.9083 | 0.8777 | 0.8102 | n.s. |

Figure 3 presents the 3D response surface plots illustrating the combined influence of arc correction and welding speed on bead geometry at a constant CTWD of 15 mm.

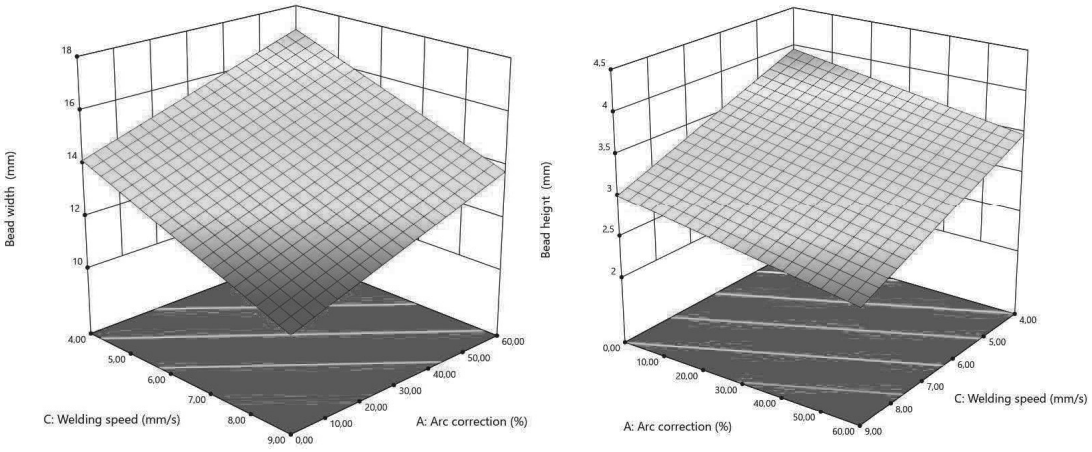



***Figure 3.*** *Response surface plots showing the influence of arc correction and welding speed on a) bead width and b) bead height at constant CTWD = 15 mm.*

The surfaces on Figure 3 reveal predominantly linear trends across the investigated parameter range, indicating a stable and predictable process behavior within the selected design space. For bead width, the developed regression model in terms of actual factors is:

$$Bead\ width = 16.34024 + 0.047917 \cdot A + 0.027500 \cdot B - 0.648000 \cdot C \quad (2)$$

where $A$ represents arc correction (%), $B$ is CTWD (mm), and $C$ is welding speed (mm/s). The model confirms that welding speed has the strongest negative influence on bead width, while arc correction contributes positively, resulting in wider beads at higher arc energy conditions. The relatively small coefficient associated with CTWD is consistent with its statistically weaker contribution in the linear model. For bead height, the regression equation in actual factors is:

$$Bead\ height = 3.25 - 0.2387 \cdot A - 0.1975 \cdot B - 0.4713 \cdot C \quad (3)$$

The response surface on Figure 3 b) demonstrates that bead reinforcement decreases with increasing welding speed and arc correction. Welding speed again shows the dominant effect, confirming that higher travel speeds reduce material accumulation and reinforcement height due to reduced energy

input per unit length. Compared to bead width, bead height exhibits a more uniform gradient, indicating a more proportionally distributed parameter influence. Overall, the response surfaces in Figure 3 confirm that welding speed is the primary governing factor for bead geometry, while arc correction provides secondary modulation of heat distribution and melt pool shape. The predominantly planar nature of the surfaces further supports the adequacy of the linear model within the investigated parameter range. Figure 4 presents the three-dimensional response surface plots for: a) heat input, b) measured voltage, and c) depth of penetration as a function of the investigated pulsed GMAW parameters.

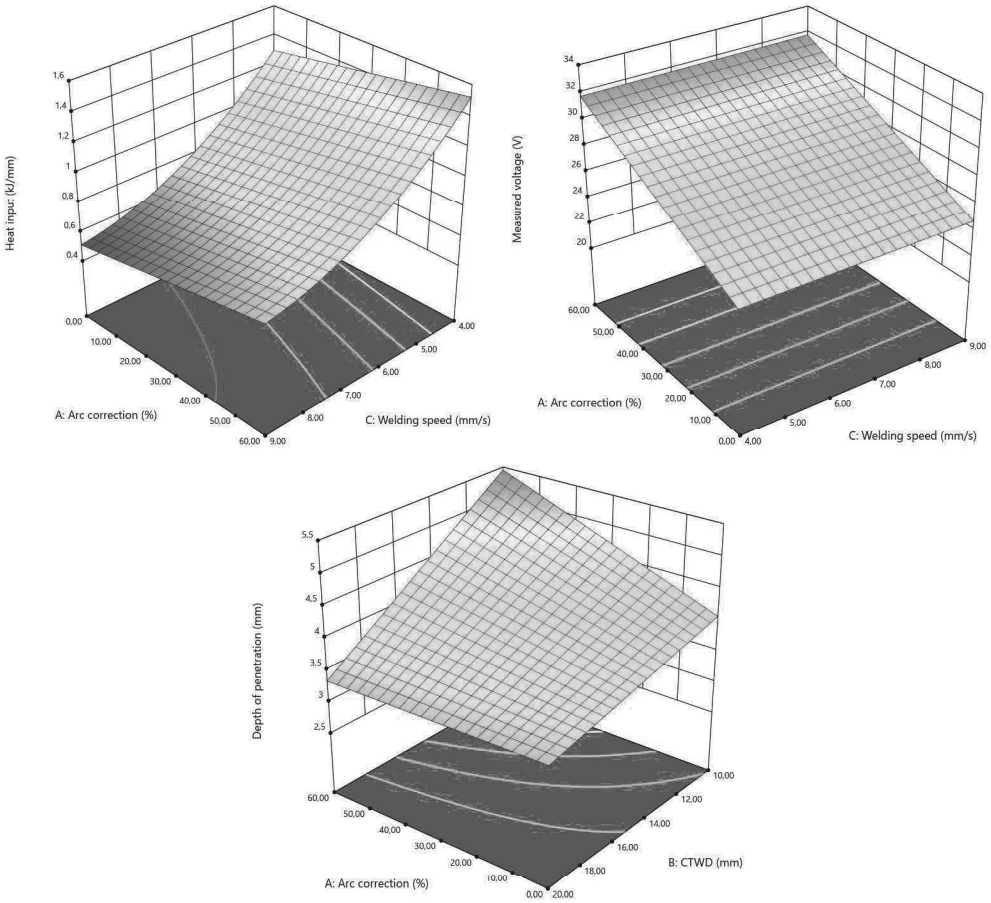



***Figure 4.*** *Three-dimensional response surface plots showing the influence of pulsed GMAW process parameters on a) heat input (CTDW =15), b) measured voltage (CTDW =15), and c) depth of penetration (welding speed = 6.5 mm/s)*

For heat input, the reduced quadratic regression model in terms of actual factors is expressed as:

$$Heat\ input = 0.8698 + 0.1132 \cdot A + 0.0543 \cdot B - 0.3910 \cdot C + 0.1481 \cdot C^2 \quad (4)$$

where *A* is arc correction (%), *B* is CTWD (mm), and *C* is welding speed (mm/s). The response surface on Figure 4a clearly demonstrates that welding speed exerts the dominant influence, with increasing travel speed significantly reducing heat input per unit length. The presence of the quadratic term ($C^2$) indicates slight curvature in the response, particularly at lower travel speeds, confirming non-linear thermal behavior within the investigated range. For measured voltage, the linear regression model in actual factors is:

$$Measured\ voltage = 28.23 + 3.51 \cdot A + 1.67 \cdot B + 0.0147 \cdot C \quad (5)$$

The response surface on Figure 4 b) indicates a strong dependence on arc correction, which is expected given that arc correction directly modifies arc characteristics and voltage stabilization. CTWD also contributes positively, reflecting the increased electrical resistance and arc length effects at larger electrode extensions. Welding speed shows a negligible influence, consistent with the statistical insignificance observed in the ANOVA results, Table 4. The results clearly indicate that, due to the strong influence of CTWD on arc voltage and resistive wire heating, the use of nominal process parameters may lead to inaccurate heat input estimations; therefore, real-time voltage measurement is essential for reliable process modelling and interpretation. Furthermore, depth of penetration was modeled using a reduced two-factor interaction (2FI) model:

$$Penetration = 4.06 + 0.3337 \cdot A - 0.6963 \cdot B - 0.4850 \cdot C - 0.3575 \cdot AB \quad (6)$$

The response surface on Figure 4c illustrates that penetration increases with higher arc correction but decreases with increasing CTWD and welding speed. CTWD exhibits the strongest negative coefficient, confirming its major role in controlling arc energy concentration and heat transfer to the base material. The significant interaction term ($A \times B$) indicates that the combined adjustment of arc correction and CTWD modifies the effective arc behavior and penetration depth beyond their individual linear contributions. Overall, the response surfaces confirm that thermal input and fusion characteristics are governed by the combined interaction of arc correction, CTWD, and welding speed. While welding speed primarily controls heat input, CTWD plays a critical role in penetration behavior, and arc correction predominantly affects arc stability and voltage response.

The observed surface trends are fully consistent with the statistical significance and model adequacy indicators obtained from the ANOVA analysis, Table 4. The obtained results reveal a coupled thermo-electrical–geometrical relationship between the investigated pulsed GMAW parameters. Measured voltage is primarily governed by arc correction, but CTWD also exhibits a statistically significant positive contribution. This confirms that increasing electrode extension modifies arc length and electrical resistance, directly influencing arc voltage even when welding speed remains unchanged. An increase in CTWD promotes resistive heating along the extended electrode length, leading to partial energy dissipation before arc impingement, reduced effective current density at the weld pool, and consequently lower penetration efficiency despite higher measured voltage levels. In contrast, welding speed does not significantly affect voltage, which is consistent with the electrical nature of arc stabilization in pulsed GMAW. Heat input is dominantly controlled by welding speed, as reflected by its strong negative coefficient and significant quadratic term. This indicates that energy per unit length is highly sensitive to travel speed variations, particularly at lower speeds where curvature effects become evident. However, since voltage is simultaneously influenced by both arc correction and CTWD, heat input is indirectly modulated by these parameters as well, demonstrating the interconnected nature of the thermal response. Penetration depth exhibits a different governing mechanism. While higher arc correction increases penetration due to enhanced arc energy concentration, CTWD shows the strongest negative effect, indicating that increased electrode extension reduces effective heat transfer to the base material despite higher voltage levels. Furthermore, the significant A×B interaction term confirms that penetration is not controlled independently by arc correction and CTWD, but rather by their combined influence on arc characteristics and melt pool behavior. This interaction-driven control mechanism would not be observable through single-factor analysis. When the responses are considered collectively, a consistent process hierarchy emerges: welding speed primarily regulates global thermal input, arc correction controls arc intensity and voltage response, while CTWD acts as a critical parameter for penetration efficiency and energy concentration. The simultaneous statistical modeling of voltage, heat input, penetration, and bead geometry therefore provides an integrated understanding of how electrical, thermal, and geometrical phenomena interact in pulsed GMAW. Unlike conventional studies that treat bead width, reinforcement, or penetration separately, the present work demonstrates that penetration behavior cannot be explained solely by heat input magnitude; instead, it depends strongly on the redistribution of arc energy governed by CTWD and its interaction with arc

correction. This integrated response surface approach thus enables predictive multi-response process tuning and reveals interaction mechanisms that remain hidden in single-response or purely empirical analyses. These findings are particularly relevant for WAAM applications, where control of penetration and bead spreading directly affects layer stacking stability.

## 4. Conclusion

This study systematically investigated the influence of arc correction, CTWD, and welding speed on thermal input, electrical response, and weld bead geometry in pulsed GMAW using response surface methodology. The developed regression models demonstrated high statistical significance ($p < 0.0001$), strong predictive capability, and non-significant lack of fit, confirming their reliability within the investigated parameter space. Welding speed was identified as the dominant parameter governing global thermal behavior, exerting the strongest influence on heat input as well as bead width and reinforcement. The presence of a significant quadratic term in the heat input model indicates non-linear thermal sensitivity at lower travel speeds. Arc correction primarily controlled measured voltage and contributed positively to penetration depth, reflecting its direct influence on arc energy distribution. CTWD, although showing a moderate influence on bead width, proved to be the most critical parameter for penetration control, exhibiting the strongest negative effect on fusion depth.

A key finding of this study is the statistically significant interaction between arc correction and CTWD in the penetration model. This interaction demonstrates that penetration depth cannot be explained solely by heat input magnitude, but rather by the combined modification of arc characteristics and energy concentration in the weld pool. Such interaction-driven behavior would not be detectable through single-factor or purely empirical analyses. Increasing CTWD enhances resistive heating along the electrode extension, redistributing energy away from the arc root and reducing effective penetration efficiency despite higher measured voltage.

The novelty of this work lies in the integrated multi-response modeling approach, where electrical (voltage), thermal (heat input), and geometrical (bead dimensions and penetration) responses were analyzed simultaneously within a unified experimental design. By linking these responses through statistically validated regression models, the study reveals how parameter interactions govern fusion efficiency and melt pool behavior in pulsed GMAW. The developed models therefore provide a predictive framework that enables systematic process optimization, reduces experimental trial-and-error, and supports data-driven control of weld bead geometry in industrial applications.

## Acknowledgments

This work was supported by the European Union under the NextGenerationEU in-strument, through the Recovery and Resilience Mechanism, within the institutional research project AIMTECH 4.5 (IP-UNIST-07), implemented by the Ministry of Science, Education and Youth of the Republic of Croatia.

## References

[1] Gojić, M., 2008. Tehnike spajanja i razdvajanja materijala. Metalurški fakultet Sveučilišta u Zagrebu, Sisak

[2] O'Brien, A. (Ed.), 2004. Welding Handbook - Welding Processes, Part 1, American Welding Society.

[3] Dinovitzer, M. et al., 2019. Effect of wire and arc additive manufacturing (WAAM) process parameters on bead geometry and microstructure. Additive Manufacturing, 26, 138–146.

[4] Kim, I.S. et al., 2003. A study on relationship between process variables and bead penetration for robotic CO2 arc welding. Journal of Materials Processing Technology, 136 (1–3), 139–145.

[5] Manikya Kanti, K., Srinivasa Rao, P., 2008. Prediction of bead geometry in pulsed GMA welding using back propagation neural network. Journal of Materials Processing Technology, 200 (1–3), 300–305.

[6] Kumar, A., Maji, K., 2020. Selection of Process Parameters for Near-Net Shape Deposition in Wire Arc Additive Manufacturing by Genetic Algorithm. Journal of Materials Engineering and Performance, 29 (5), 3334–3352.

[7] Krolo, J., Bilušić, M., Radić, S., 2024. Analysis of the resistance spot welding process of stainless-steel using response surface methodology and surface topography analysis. Proceedings of the 13th International Conference Mechanical Technologies and Structural Materials 2024 (MTSM 2024), Split, Croatia, 217–224.

[8] Krolo, J., Lela, B., Grgić, K., Jozić, S., 2022. Production of Closed-Cell Foams out of Aluminum Chip Waste: Mathematical Modeling and Optimization. Metals, 12 (6), 933.

[9] Krolo, J., Špada, V., Bilušić, M., Čatipović, N., 2025. Welding of Solid-State-Recycled Aluminum Alloy: Comparative Analysis of the Mechanical and Microstructural Properties. Applied Sciences, 15 (3), 1222.